

First-passage Brownian functionals with stochastic resetting

Prashant Singh¹ and Arnab Pal²

¹International Centre for Theoretical Sciences, Tata Institute of Fundamental Research, Bengaluru 560089, India

²The Institute of Mathematical Sciences, CIT Campus, Taramani, Chennai 600113, India & Homi Bhabha National Institute, Training School Complex, Anushakti Nagar, Mumbai 400094, India

E-mail: prashant.singh@icts.res.in; arnabpal@imsc.res.in

Abstract. We study the statistical properties of first-passage time functionals of a one dimensional Brownian motion in the presence of stochastic resetting. A first-passage functional is defined as $V = \int_0^{t_f} Z[x(\tau)]$ where t_f is the first-passage time of a reset Brownian process $x(\tau)$, i.e., the first time the process crosses zero. In here, the particle is reset to $x_R > 0$ at a constant rate r starting from $x_0 > 0$ and we focus on the following functionals: (i) local time $T_{loc} = \int_0^{t_f} d\tau \delta(x - x_R)$, (ii) residence time $T_{res} = \int_0^{t_f} d\tau \theta(x - x_R)$, and (iii) functionals of the form $A_n = \int_0^{t_f} d\tau [x(\tau)]^n$ with $n > -2$. For first two functionals, we analytically derive the exact expressions for the moments and distributions. Interestingly, the residence time moments reach minima at some optimal resetting rates. A similar phenomena is also observed for the moments of the functional A_n . Finally, we show that the distribution of A_n for large A_n decays exponentially as $\sim \exp(-A_n/a_n)$ for all values of n and the corresponding decay length a_n is also estimated. In particular, exact distribution for the first passage time under resetting (which corresponds to the $n = 0$ case) is derived and shown to be exponential at large time limit in accordance with the generic observation. This behavioural drift from the underlying process can be understood as a ramification due to the resetting mechanism which curtails the undesired long Brownian first passage trajectories and leads to an accelerated completion. We confirm our results to high precision by numerical simulations.

1. Introduction

Brownian functionals appear ubiquitously in many different disciplines spanning across physics, stochastic processes, finance, computer science and mathematics (see [1] for a comprehensive review of this topic). The celebrated Feynman-Kac formalism has been instrumental to understand the statistical properties of the functionals of a one-dimensional Brownian motion by translating the classical diffusion problems to the quantum mechanics [2]. Study of such Brownian functionals also appears in stochastic thermodynamics in the form of fluctuation theorems which express universal properties

of the statistical distribution for functionals like work, heat or entropy change, evaluated along the fluctuating trajectories taken from ensembles with some well specified initial distributions [3, 4]. In this paper, we focus on another class of functionals that has also attracted quite a lot of attention, namely the “first-passage Brownian functionals”. More precisely, let us consider a diffusive particle in one dimension whose position $x(\tau)$ is governed by the following equation of motion

$$\frac{dx}{d\tau} = \eta(\tau), \quad (1)$$

where $\eta(\tau)$ is the Gaussian white noise with zero mean and correlation $\langle \eta(\tau)\eta(\tau') \rangle = 2D\delta(\tau - \tau')$. Here, D is the diffusion coefficient. The particle is initially located at $x_0 > 0$. Moreover, we consider that there is an absorbing boundary at the origin and let t_f denote the first-passage time of the Brownian particle to the origin starting from position x_0 . Clearly t_f is a random variable and fluctuates between realizations. A functional constructed along such a trajectory

$$V = \int_0^{t_f} Z[x(\tau)]d\tau, \quad (2)$$

is thus random and defined as a first passage functional [1]. Here, $Z(x)$ can, in principle, be an arbitrary function of x . Given this form, one is usually interested in the various statistical properties of the functional V .

A well-studied Brownian functional in the literature is the local time for which $Z(x) = \delta(x - x_\ell)$. It measures the total time that the particle spends in the vicinity of a desired location x_ℓ in space [1, 5–10]. As such, the local time provides interesting information with regard to the spatio-temporal properties of the particle’s trajectory and is thus a useful measure with various applications in chemical reactions and catalytic processes [11–14]. Another example of such functional is the residence or occupation time which characterizes the total time that the particle spends in a given region of space [15]. For instance, the celebrated “arcsine law” of Lévy describes the probability distribution of the time spent by a one dimensional Brownian particle on the positive side of the origin out of the total given time t [1, 5, 16]. For this class of functionals, $Z(x) = \theta(x - x_\ell)$, where $\theta(x - x_\ell)$ denotes the Heaviside function. In the past, the residence time has been studied in various different scenarios such as diffusion in confinement [17], or in a potential landscape [18], in heterogeneous diffusion processes [19], in Brownian excursion processes [20] and active models [21]. While these studies have mostly considered residence time for fixed time, we here focus on a situation where the residence time is estimated upto the first passage event. Another generic functional that has been extensively studied is of the form $Z(x) = x^n$ where n is some real number. This observable has been studied both in the context of fixed time [1] or random time ensemble [22, 23]. In particular, for $n = 0$ in Eq. (2), V simply represents the first-passage time t_f which has a myriad of applications in all fields (see [16, 24] for pedagogic introduction and applications of first passage processes). Similarly for

$n = 1$ in Eq. (2), V represents the total area swept by the diffusing particle till its first-passage time. The study of this area has found applications in sandpile models, percolation models and queueing theory [23, 25–28]. In compact directed percolation on square lattice, the area of the staircase polygon is related to the $n = 1$ case [23, 26] whereas in queueing theory this area is related to the cumulative waiting-time experienced by the customers during busy period [25]. The first-passage area has also been studied in a one-dimensional jump-diffusion process [29], drifted Brownian motion [30], Lévy process [31] and Ornstein-Uhlenbeck process [32, 33]. The case $n = -\frac{3}{2}$ was shown to represent the lifetime of a comet within the ambit of random walk theory [34]. The case $n = -\frac{1}{2}$ is related to the period of oscillation of a particle in disordered systems modeled by Sinai potential [35]. We refer to [1] for a review on the applications of these “first passage Brownian functionals” for the *reset-free processes*. In this work, our central goal is to extend our understanding of first passage Brownian functionals in the presence of stochastic resetting [36–38]. As we will see, resetting has significant effects on the dynamics which results in non-trivial and distinct changes in the statistics of first-passage time observables.

Stochastic resetting is a renewal process where the dynamics is repeated after some random or fixed time. Although very simple to describe, this mechanism is in fact quite natural to many processes around us. For example, unbinding events in a chemical reaction [39, 40], cleavage in RNA polymerization [41] or dissociation kinetics of GTP-RhoA in cell contraction [42] can be understood as resetting events. The phenomena has been catalyzed even further since over the last decade, resetting has found overreaching applications in statistical physics [43–52], computer science [53, 54], ecology [55–57], complex systems [58–60] operation research [61–63] and economics [64–66]. Recently, the field has also seen advancements in experiments [67–69]. A paradigm model in the field is the Brownian motion with stochastic resetting for which many interesting results exist [47, 70–76]. We refer to [36] for a review on the state of the art of the subject and [77] for a perspective on its connection with the inspection paradox. In particular, the latter pinpoints to how/when stochastic resetting expedites completion of arbitrary stochastic processes.

The essential idea that stochastic trajectories governed by resetting dynamics share is the following: Consider a particle whose position $x(t)$ evolves according to Eq. (1) starting from $x(0) = x_0 (> 0)$. Motion of the particle is then stopped intermittently at a rate r and it is instantaneously brought to a position $x_R (> 0)$. Following the resetting event, the particle starts diffusing again until the next resetting event occurs. The microscopic evolution equation for the particle can then be written as

$$x(t + \Delta t) = \begin{cases} x(t) + \eta(t)\Delta t, & \text{with prob } (1 - r\Delta t), \\ x_R, & \text{with prob } r\Delta t. \end{cases} \quad (3)$$

where recall that $\eta(t)$ is the Gaussian white noise with zero mean and variance $\langle \eta(t)\eta(t') \rangle = 2D\delta(t - t')$. For simplicity, we set $D = \frac{1}{2}$ without any loss of generality. Moreover, we will assume that there is an absorbing boundary at the origin, and the

process ends as soon as the particle hits the boundary. As in the reset-free process, we will denote the first passage time under resetting also by t_f . Our aim is to investigate the statistical properties of the functional in Eq. (2) for the motion that is governed by Eq. (3). It is important to note that numerous studies have been made on t_f unraveling many key features: expedition of the first-passage time process perhaps being the most remarkable one [36–38, 78–81]. For example, it is known that the moments of area functional for simple diffusion ($r = 0$ case) are infinite [22, 23]. This is a natural consequence of the fact that the first passage time density for the simple diffusion has a power law tail at large time [16]. In contrast, first passage time density of a reset Brownian process falls exponentially at large times [36, 48]. So, one would expect that the area will attain finite moments under the resetting mechanism. These crucial observations serve as a motivation for us to extend the Feynman-Kac framework to the first passage Brownian functionals in the presence of resetting. In particular, we provide a comprehensive analysis of the following functionals:

- (i) *Local time*: The first functional that we consider is the local time T_{loc} which refers to the amount of time (density) spent in the neighbourhood of position x_ℓ till its first-passage time. For this case, $Z(x) = \delta(x - x_\ell)$ and thus $T_{loc}(x_\ell) = \int_0^{t_f} d\tau \delta(x(\tau) - x_\ell)$. In here, we will set $x_\ell = x_R$ so that we would be measuring the local time near the resetting location.
- (ii) *Residence time*: The second observable goes under the name occupation/residence time for which $Z(x) = \theta(x - x_R)$ with $\theta(y)$ being the Heaviside theta function. Thus, the residence time takes the form $T_{res}(x_R) = \int_0^{t_f} d\tau \theta(x(\tau) - x_R)$ and estimates the cumulative time spent by the particle in the region $x > x_R$ till its absorption at the origin.
- (iii) Finally, we look at a class of functionals with $Z(x) = x^n$ for $n > -2$. We denote them by $A_n(x_0) = \int_0^{t_f} d\tau [x(\tau)]^n$. We keep x_0 in the argument to indicate the initial position. Our focus would be to understand the consequences of resetting on the distribution and moments of $A_n(x_0)$.

For the convenience of the readers, we provide a short outline of the paper in the following. In Sec. 2, we derive a backward differential equation for the moment generating function of $V(x_0)$. Deploying this backward equation, we then study local time in Sec. 3, residence time in Sec. 4 and functional $A_n(x_0)$ in Sec. 5. Finally, we conclude with some future outlook in Sec. 6.

2. General formulation

In this section, we show how to compute the probability distribution function (PDF) $P_R(V, x_0)$ of a Brownian functional V over the time interval $[0, t_f]$ where t_f is the first-passage time of the process in the presence of stochastic resetting. Our starting point would be to derive a differential equation for the moment generating function defined

as follows

$$Q(p, x_0) = \int_0^\infty dV e^{-pV} P_R(V, x_0), \quad (4)$$

$$= \langle e^{-p \int_0^{t_f} Z[x(\tau)] d\tau} \rangle, \quad (5)$$

where the average $\langle \dots \rangle$ in the second line denotes averaging over all trajectories as well as over t_f . This enables us to compute the moments of V as

$$\langle V^m \rangle = (-1)^m \left(\frac{\partial^m Q(p, x_0)}{\partial p^m} \right) \Big|_{p \rightarrow 0}. \quad (6)$$

We would like to construct now a backward differential equation for $Q(p, x_0)$. To proceed, consider a typical trajectory $\{x(\tau); 0 \leq \tau \leq t_f\}$ that starts from $x_0 > 0$ at $\tau = 0$ and split into two parts: (i) a left interval $[0, \Delta t]$ and (ii) a right interval $[\Delta t, t_f]$ with $\Delta t \rightarrow 0$. In the first interval, the position of the particle changes from x_0 to $x'_0 = x_0 + \Delta x$ (where the exact form of Δx will be specified later). Starting from this new position x'_0 at time Δt , the particle reaches the origin at time t_f . This path-decomposition leads us to break the integration in Eq. (5) as $\int_0^{t_f} = \int_0^{\Delta t} + \int_{\Delta t}^{t_f}$ and in the limit $\Delta t \rightarrow 0$, we get

$$\begin{aligned} Q(p, x_0) &= \langle e^{-pZ(x_0)\Delta t} e^{-p \int_{\Delta t}^{t_f} Z[x(\tau)] d\tau} \rangle, \\ &= \langle e^{-pZ(x_0)\Delta t} Q(p, x'_0) \rangle. \end{aligned} \quad (7)$$

To evaluate x'_0 , note that starting from the initial position x_0 , in small time Δt , the particle can either move to $x_0 + \eta(0)\Delta t$ with probability $(1 - r\Delta t)$ or reset to x_R with probability $r\Delta t$. Taking contributions from both, we have

$$\begin{aligned} x'_0 &= x_0 + \eta(0)\Delta t, & \text{with probability } (1 - r\Delta t), \\ &= x_R, & \text{with probability } r\Delta t \end{aligned} \quad (8)$$

We now use Eq. (8) in Eq. (7) along with the noise properties $\langle \eta(0) \rangle = 0$ and $\langle \eta^2(0) \rangle = 1/\Delta t$ as $\Delta t \rightarrow 0$. Keeping only the leading order terms in Δt we get the following backward equation in the presence of resetting

$$\frac{1}{2} \frac{\partial^2 Q(p, x_0)}{\partial x_0^2} - pZ(x_0)Q(p, x_0) - rQ(p, x_0) + rQ(p, x_R) = 0. \quad (9)$$

Eq. (9) is the central equation of the paper. Notice simply that it boils down to the result (see Eq. (51)) in [1] for $r = 0$. The above equation is valid in the domain $[0, \infty]$ and we need to supplement appropriate boundary conditions to solve it

$$Q(p, x_0 \rightarrow 0^+) = 1, \quad (10)$$

$$Q(p, x_0 \rightarrow \infty) < \infty. \quad (11)$$

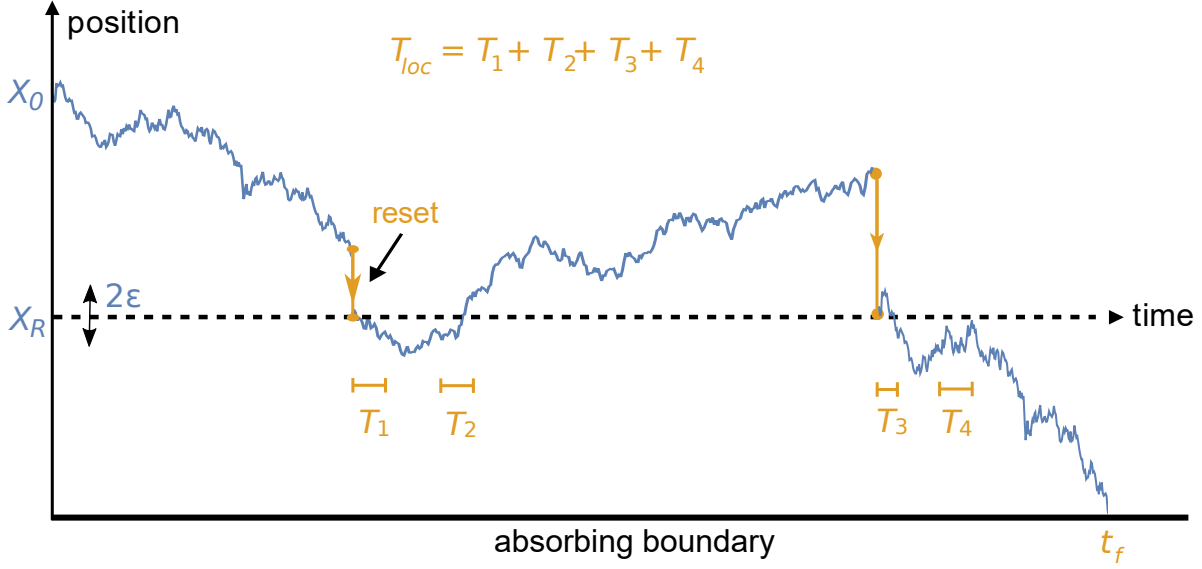


Figure 1. Schematic of local time of diffusion with stochastic resetting. Local time T_{loc} is a collection of all time segments in the trajectory (as shown in the plot) spent by the particle in the domain 2ϵ around x_R upto the first passage time t_f .

The first boundary condition is easy to understand since the particle will be absorbed momentarily if it starts from the origin. This means that the first-passage time $t_f \rightarrow 0$ (hence the integral $V = \int_0^{t_f} d\tau Z[x(\tau)] \rightarrow 0$) and from Eq. (5) one derives Eq. (10). Let us now look at the second boundary condition. Although the particle is initially at $x_0 \rightarrow \infty$, the next resetting event can bring it to the finite location x_R within a finite time window. Therefore, the first-passage time t_f is typically finite for any non-zero and finite value of r . Based on this intuition, we expect the functional V to remain finite. This results in the boundary condition in Eq. (11).

So, given a functional $Z(x)$, the scheme would be to first solve the backward equation Eq. (9) with the appropriate boundary conditions mentioned above to obtain $Q(p, x_0)$ explicitly and then invert the Laplace transform in Eq. (5) to get the desired PDF $P_R(V, x_0)$ of the first-passage functional. In the following sections, we discuss various choices of $Z(x)$ as mentioned in Sec. 1 and illustrate the consequences of resetting.

3. Local time

The local time density spent by the particle at position x_ℓ upto the first-passage time t_f is given by

$$T_{loc}(x_\ell) = \int_0^{t_f} d\tau \delta[x(\tau) - x_\ell] . \quad (12)$$

The appearance of the delta function in the above definition is understood in the following limiting sense:

$$T_{loc}(x_\ell) = \lim_{\epsilon \rightarrow 0} \frac{T_{2\epsilon}(x_\ell)}{2\epsilon}, \quad \text{where } T_{2\epsilon}(x_\ell) = \int_0^{t_f} d\tau [\theta(x(\tau) - x_\ell - \epsilon) - \theta(x(\tau) - x_\ell + \epsilon)]. \quad (13)$$

In what follows, such regularization procedure should precede every use of the delta function, but we will omit it for brevity. Clearly, $T_{2\epsilon}(x_\ell)$ measures the total time spent by the particle inside the box $[x_\ell - \epsilon, x_\ell + \epsilon]$ till time t_f in the presence of resetting. Thus, by definition, the normalization condition reads $\int_0^\infty T_{loc}(x_\ell) dx_\ell = t_f$. Here, we are interested in estimating the local time density near the resetting location x_R [see Fig. 1]. Thus, using $Z(x) = \delta(x - x_R)$ from Eq. (12) and substituting into the backward Eq. (9), we obtain

$$\frac{1}{2} \frac{\partial^2 Q(p, x_0)}{\partial x_0^2} - p \delta(x_0 - x_R) Q(p, x_0) - rQ(p, x_0) + rQ(p, x_R) = 0. \quad (14)$$

For $x_0 \neq x_R$, we get rid of the term with $\delta(x_0 - x_R)$ and rewrite Eq. (14) as

$$\frac{1}{2} \frac{\partial^2 Q(p, x_0)}{\partial x_0^2} - rQ(p, x_0) + rQ(p, x_R) = 0. \quad (15)$$

It is easy to solve this equation and get the solutions

$$Q(p, x_0) = \begin{cases} \mathcal{A}e^{\sqrt{2r}x_0} + \mathcal{B}e^{-\sqrt{2r}x_0} + Q(p, x_R), & \text{for } x_0 < x_R, \\ \mathcal{C}e^{\sqrt{2r}x_0} + \mathcal{D}e^{-\sqrt{2r}x_0} + Q(p, x_R), & \text{for } x_0 > x_R. \end{cases} \quad (16)$$

Here, the functions \mathcal{A} , \mathcal{B} , \mathcal{C} and \mathcal{D} are independent of x_0 but may depend on x_R and p . To evaluate these functions, we need to specify four conditions on $Q(p, x_0)$. Two of these conditions come from the behaviour of $Q(p, x_0)$ as $x_0 \rightarrow 0^+$ and $x_0 \rightarrow \infty$ which are, respectively, written in Eqs. (10) and (11). In addition, we use two matching conditions. To see these, we first integrate Eq. (14) from $x_0 = x_R - \delta$ to $x_0 = x_R + \delta$ and take $\delta \rightarrow 0^+$. Next, we use the continuity of $Q(p, x_0)$ across $x_0 = x_R$. The resultant conditions are

$$Q(p, x_R^+) = Q(p, x_R^-), \quad (17)$$

$$\left(\frac{\partial Q}{\partial x_0} \right)_{x_R^+} - \left(\frac{\partial Q}{\partial x_0} \right)_{x_R^-} = 2pQ(p, x_R). \quad (18)$$

We can now evaluate the functions \mathcal{A} , \mathcal{B} and \mathcal{D} and plug them in Eq. (16) to obtain the exact form of $Q(p, x_0)$. However, since we are interested in the case $x_0 = x_R$, it is easy to see from Eq. (16) that $Q(p, x_R)$ is completely characterised by $\mathcal{D}(x_R, p)$ which reads

$$\mathcal{D}(x_R, p) = \frac{\sqrt{r} [Q(p, x_R) - 1] - \sqrt{2p} Q(p, x_R) \sinh(\sqrt{2r}x_R)}{\sqrt{2} [p \sinh(\sqrt{2r}x_R) - \sqrt{r}]} e^{\sqrt{2r}x_R}. \quad (19)$$

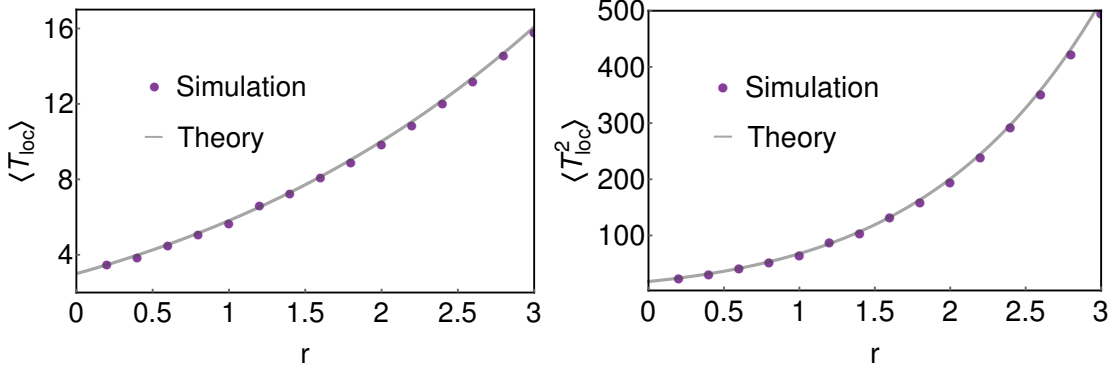


Figure 2. Comparison of the first two moments of T_{loc} for Brownian motion in Eq. (21) with numerical simulation. We have set $x_0 = x_R = 1.5$ for both the plots.

Substituting this into the second line of Eq. (16) yields

$$Q(p, x_R) = \frac{\sqrt{r}}{\sqrt{r} + \sqrt{2}p \sinh(\sqrt{2r}x_R)}. \quad (20)$$

To get the form of the distribution of T_{loc} , one has to perform the inverse Laplace transformation of Eq. (20). Before this, let us look at the moments of T_{loc} using Eq. (6). Inserting $Q(p, x_R)$ from Eq. (20) in Eq. (6), we find that the m -th order moment of T_{loc} is given by

$$\langle T_{loc}^m \rangle = m! \left[\sqrt{\frac{2}{r}} \sinh(\sqrt{2r}x_R) \right]^m. \quad (21)$$

In Fig. 2, we have plotted the first two moments of T_{loc} and compared them against the simulation. We observe an excellent agreement of our analytical results with the simulation. From Eq. (21), we find that the local time scales as $T_{loc} \sim \frac{1}{\sqrt{r}} \exp(\sqrt{2r}x_R)$ for large r which is different than $T_{loc} \sim x_R$ scaling without resetting. As r increases, the particle is brought to x_R more frequently which causes it to spend more time in the vicinity of x_R . This results in the enhancement of the local time for non-zero r .

Returning to the distribution of T_{loc} , we next perform the inverse Laplace transformation of $Q(p, x_R)$ in Eq. (20) and obtain

$$P_R(T_{loc}, x_R) = \frac{\sqrt{r}}{\sqrt{2} \sinh(\sqrt{2r}x_R)} \exp\left(-\frac{\sqrt{r}}{\sqrt{2} \sinh(\sqrt{2r}x_R)} T_{loc}\right). \quad (22)$$

In Fig. 3(a), we have plotted $P_R(T_{loc}, x_R)$ and compared with the results of numerical simulations. The distribution $P_R(T_{loc}, x_R)$ decays exponentially with decay length equal to $\sqrt{2} \sinh(\sqrt{2r}x_R) / \sqrt{r}$. Since the typical value of T_{loc} increases with r , the decay length also increases with r .

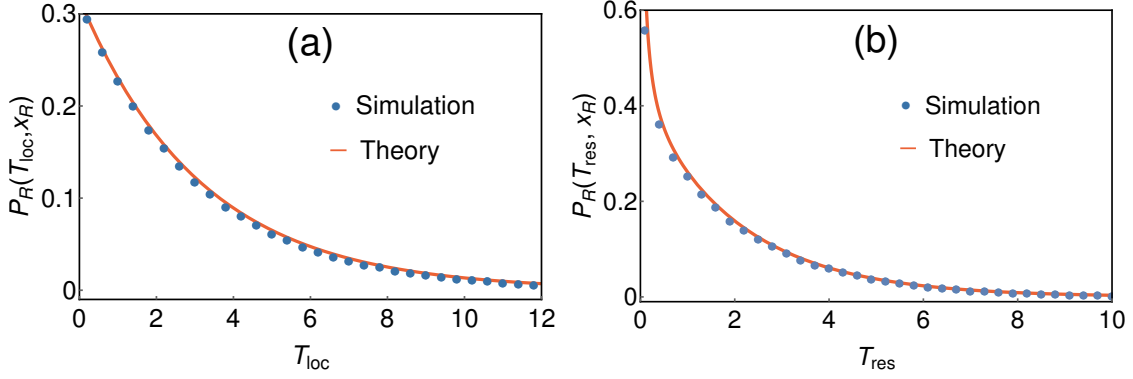


Figure 3. (a) Theoretical plot of $P_R(T_{loc}, x_R)$ (Eq. (22)) and its comparison with the numerical simulations. Parameters chosen are $x_0 = x_R = 1$ and $r = 1.5$. (b) Comparison of the residence time distribution $P_R(T_{res}, x_R)$ in Eq. (33) with the numerical simulation. Here, we have set $x_0 = x_R = 1$ and $r = 2$.

4. Residence time

In this section, we discuss the effects of resetting on the statistics of residence/occupation time T_{res} . We define residence time as the cumulative time that particle spends in the region $x > x_R$ before getting absorbed at the origin, thus $T_{res} = \int_0^{t_f} d\tau \theta(x(\tau) - x_R)$ [see Fig. 4]. Substituting $Z(x) = \theta(x - x_R)$ into Eq. (9), we get

$$\frac{1}{2} \frac{\partial^2 Q(p, x_0)}{\partial x_0^2} - p\theta(x_0 - x_R)Q(p, x_0) - rQ(p, x_0) + rQ(p, x_R) = 0. \quad (23)$$

Solving this equation separately for $x_0 \geq x_R$ (for which $\theta(x_0 - x_R) = 1$) and $x_0 < x_R$ (for which $\theta(x_0 - x_R) = 0$), we get

$$Q(p, x_0) = \begin{cases} \mathcal{C}_1 e^{\sqrt{2r}x_0} + \mathcal{C}_2 e^{-\sqrt{2r}x_0} + Q(p, x_R), & \text{for } x_0 < x_R, \\ \mathcal{C}_3 e^{\sqrt{2r}x_0} + \mathcal{C}_4 e^{-\sqrt{2r}x_0} + \frac{r}{r+p} Q(p, x_R), & \text{for } x_0 > x_R. \end{cases} \quad (24)$$

The constants \mathcal{C}_1 , \mathcal{C}_2 , \mathcal{C}_3 and \mathcal{C}_4 are independent of x_0 but are, in general, functions of p and x_R . To compute them, we use the boundary conditions in Eqs. (10) and (11) along with the continuity conditions for $Q(p, x_0)$ and $\frac{\partial Q(p, x_0)}{\partial x_0}$ across $x_0 = x_R$

$$Q(p, x_R^+) = Q(p, x_R^-), \quad (25)$$

$$\left(\frac{\partial Q}{\partial x_0} \right)_{x_R^+} = \left(\frac{\partial Q}{\partial x_0} \right)_{x_R^-}. \quad (26)$$

Using these conditions, it is straightforward to compute all $\mathcal{C}(p, x_R)$ functions in Eq. (24). However, once again, we are interested in the case where $x_0 = x_R$. For this, we need to specify only the expression of $\mathcal{C}_4(p, x_R)$ as indicated by the second line in Eq. (24) [$\mathcal{C}_3(p, x_R) = 0$ from Eq. (11)]. The expression of $\mathcal{C}_4(p, x_R)$ reads

$$\mathcal{C}_4(p, x_R) = \frac{[1 - Q(p, x_R)](p+r) + p Q(p, x_R) \cosh(\sqrt{2r}x_R)}{(p+r) \left[\cosh(\sqrt{2r}x_R) - \sqrt{\frac{p+r}{r}} \sinh(\sqrt{2r}x_R) \right]} e^{\sqrt{2(r+p)}x_R}. \quad (27)$$

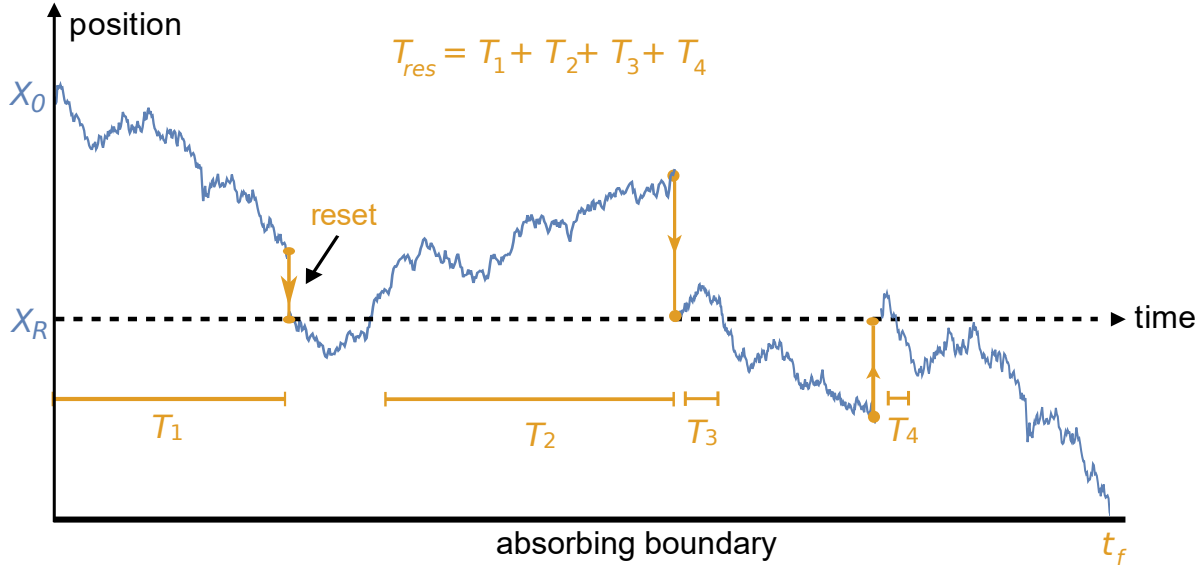


Figure 4. Schematic of residence time of diffusion with stochastic resetting. Residence time T_{res} is a collection of all time segments in the trajectory (as shown in the plot) spent by the particle in the domain $x > x_R$ upto the first passage time t_f .

and inserting this in the second line of Eq. (24) gives

$$Q(p, x_R) = \frac{\sqrt{r(r+p)}}{\sqrt{r(r+p) + p \sinh(\sqrt{2rx_R})}}. \quad (28)$$

To summarise, we have obtained the exact form of the Laplace transformation of the distribution $P_R(T_{res}, x_R)$ from which the moments can be computed using Eq. (6). Here, we provide exact expressions for the first two moments:

$$\langle T_{res}(x_R) \rangle = \frac{\sinh(\sqrt{2rx_R})}{r}, \quad (29)$$

$$\langle T_{res}^2(x_R) \rangle = \frac{\sinh(\sqrt{2rx_R})}{r^2} \left[1 + 2 \sinh(\sqrt{2rx_R}) \right]. \quad (30)$$

These two moments are plotted in Fig. 5 where we have also performed comparison with the numerical simulations. In the limit $r \rightarrow 0$, the moments of T_{res} diverge. On the other hand, repeated resetting at a rate r renders the moments finite. Physically, this can be understood in the following way: For standard Brownian motion, there will be some trajectories for which the particle will always stay on $x > x_R$ region and avoid getting absorbed at the origin. Such trajectories contribute to $t_f \rightarrow \infty$ and $T_{res} \rightarrow \infty$. From an analysis shown later, we find that the weight of these trajectories to the distribution is $\sim 1/\sqrt{T_{res}}$. This results in the diverging moments. However, in presence of resetting, particle will be brought to x_R intermittently which will reduce drastically the effective contribution of trajectories with $t_f \rightarrow \infty$ and $T_{res} \rightarrow \infty$. Under this situation, the effective contribution of these trajectories to the probability distribution is $\sim e^{-aT_{res}}$ (see below) where a is some positive function of r and x_R . This, in turn, results in finite moments.

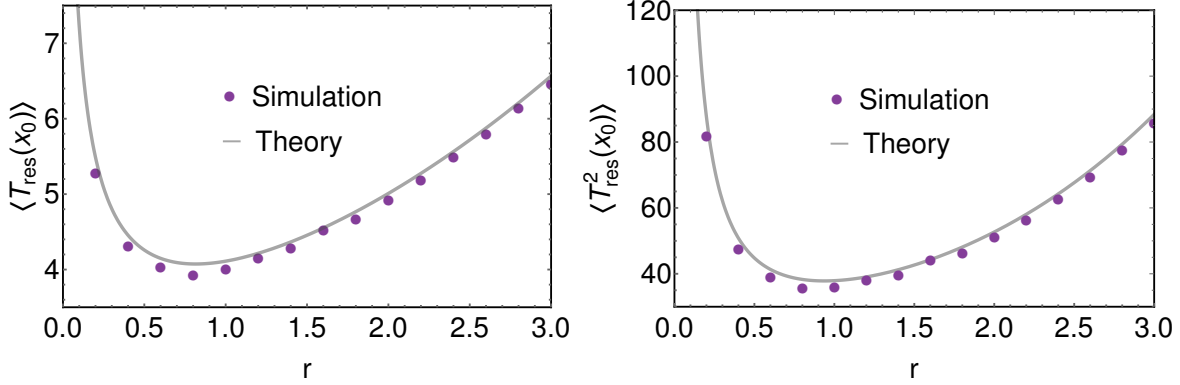


Figure 5. Comparison of the first two moments of T_{res} given by Eqs. (29) and (30) with numerical simulations. Here, we have set $x_0 = x_R = 1.5$ in both the plots.

Quite interestingly, we observe that the moments exhibit a non-monotonic behaviour with respect to r with minimum value at some optimal resetting rate r^* (see Fig. 5). We saw above that the first two moments diverge respectively as $\sim 1/\sqrt{r}$ and $\sim 1/r^{3/2}$ for $r \ll r^*$. Hence, the moments decrease with increasing r for $r \ll r^*$. On the other hand, for $r \gg r^*$, the particle is frequently reset to x_R which reduces its likelihood for a first passage to the origin. As a result, one expects the typical value of residence time T_{res} to increase with r for $r \gg r^*$. In fact, Eqs. (29) and (30) reveal that the first two moments diverge as $\sim r^{-1}e^{\sqrt{2rx_R}}$ and $\sim r^{-2}e^{2\sqrt{2rx_R}}$ respectively for $r \rightarrow \infty$. Therefore, at some $r = r^*$, the slope of the moments changes from negative to positive which essentially corresponds to their minimum value.

After analysing the moments, we next proceed to compute the distribution of T_{res} . To this end, we rewrite $Q(p, x_R)$ as

$$Q(p, x_R) = \sum_{k=0}^{\infty} \frac{(-1)^k r^{\frac{k+1}{2}}}{(\sinh(\sqrt{2rx_R}))^{k+1}} \left(\frac{\sqrt{p+r}}{p} \right)^{k+1}. \quad (31)$$

To proceed further, we use the following inverse Laplace transformation:

$$\mathcal{L}_{p \rightarrow T_{res}}^{-1} \left[\left(\frac{\sqrt{p+r}}{p} \right)^{k+1} \right] = T_{res}^{\frac{k-1}{2}} {}_1\bar{F}_1 \left(-\frac{k+1}{2}, \frac{k+1}{2}, -rT_{res} \right), \quad \text{for } k > -1, \quad (32)$$

where $\mathcal{L}_{p \rightarrow T_{res}}^{-1} [g(p)]$ denotes an inverse Laplace transformation of the function $g(p)$. Here, ${}_1\bar{F}_1(a, b, y)$ stands for the regularized confluent hypergeometric function [91]. Finally, from Eq. (31), we have

$$P_R(T_{res}, x_R) = \frac{r}{\sinh(\sqrt{2rx_R})} H(rT_{res}), \quad (33)$$

where the scaling function $H(y)$ is given by

$$H(y) = \frac{1}{\sqrt{y}} \sum_{k=0}^{\infty} \left(-\frac{\sqrt{y}}{\sinh(\sqrt{2rx_R})} \right)^k {}_1\bar{F}_1 \left(-\frac{k+1}{2}, \frac{k+1}{2}, -y \right). \quad (34)$$

In Fig. 3(b), we have plotted $P_R(T_{res}, x_R)$ and compared it with the numerical simulations to find an excellent match. To see the effect of resetting on the distribution, it is instructive to look at the asymptotic form of $H(y)$. As $y \rightarrow 0$, we have ${}_1\bar{F}_1\left(-\frac{k+1}{2}, \frac{k+1}{2}, -y\right) \simeq \frac{1}{\Gamma\left(\frac{k+1}{2}\right)}$. On the other hand for large y , we have ${}_1\bar{F}_1\left(-\frac{k+1}{2}, \frac{k+1}{2}, -y\right) \simeq \frac{(\sqrt{y})^{k+1}}{\Gamma(k+1)}$. Inserting these asymptotic forms in Eq. (34) and performing some algebraic simplifications, we find

$$H(y) \simeq \frac{1}{\sqrt{\pi y}}, \quad \text{as } y \rightarrow 0, \quad (35)$$

$$\simeq e^{-\frac{y}{\sinh(\sqrt{2rx_R})}}, \quad \text{as } y \rightarrow \infty. \quad (36)$$

Finally, substituting these forms in Eq. (33), we find that the distribution $P_R(T_{occ}, x_R)$ has the following asymptotic forms:

$$P_R(T_{res}, x_R) \simeq \frac{\sqrt{r}}{\sqrt{\pi T_{res}} \sinh(\sqrt{2rx_R})}, \quad \text{for } T_{res} \ll r^{-1}, \quad (37)$$

$$\simeq \frac{r}{\sinh(\sqrt{2rx_R})} \exp\left(-\frac{r T_{res}}{\sinh(\sqrt{2rx_R})}\right), \quad \text{for } T_{res} \gg r^{-1}. \quad (38)$$

We see that for no-resetting case, the distribution exhibits power-law decay of the form $\sim 1/\sqrt{T_{res}}$. On the other hand, in presence of resetting, the distribution has an exponential tail of the form in Eq. (38). Emergence of exponential tails is a hallmark property for observables under stochastic resetting mechanism which was first noted in the context of first passage time [37] (also see below and [48]). Here too, we observe a similar behavior which essentially results in finite moments in comparison to the underlying process.

5. Functional of the form $A_n(x_0) = \int_0^{t_f} [x(\tau)]^n d\tau$

In this section, we focus on functionals of type

$$A_n(x_0) = \int_0^{t_f} [x(\tau)]^n d\tau, \quad \text{with } n > -2. \quad (39)$$

As discussed before, $A_n(x_0)$ for different values of n arises in various contexts like search problem, queueing theory, particle in harmonic or Sinai potential. Statistics of $A_1(x_0)$ (for the $r = 0$ case) was studied in different contexts like sandpile model and directed percolation [23, 25–28]. For $r = 0$, the distribution of $A_n(x_0)$ was exactly computed in [22] for all $n > -2$. Here, we study this problem in presence of resetting. In particular, note that for $n = 0$, one has $A_0(x_0) = t_f$ which is nothing but the first-passage time of diffusion with resetting. The topic has been studied quite extensively spanning different stochastic processes that undergo resetting [36, 79–88]. However, to the best of our knowledge, the $n \neq 0$ cases have not yet been studied. This section provides a systematic understanding of the problem for general n .

As before, the starting point is to substitute the form of the function i.e., $Z(x) = x^n$ into the Eq. (9)

$$\frac{1}{2} \frac{\partial^2 Q(p, x_0)}{\partial x_0^2} - p x_0^n Q(p, x_0) - rQ(p, x_0) + rQ(p, x_R) = 0, \quad (40)$$

which is to be solved along with boundary conditions in Eqs. (10) and (11). Solving this equation for arbitrary n turns out to be difficult. Only for $n = 0$ and $n = 1$, we can exactly solve Eq. (40). For other values of n , we present some results on the moments and distribution based on heuristic analysis. In what follows, we briefly discuss the case of $n = 0$ for the sake of completeness and then look at the $n = 1$ and general $n (> -2)$ cases separately.

5.1. $n = 0$

Let us first look at the case $n = 0$ for which $A_0(x_0)$ represents the first passage time (FPT) t_f to the origin starting from x_0 . It is easy to solve Eq. (40) for this case and obtain

$$Q(p, x_0) = \mathbb{C}_1 e^{-\sqrt{2(r+p)x_0}} + \mathbb{C}_2 e^{\sqrt{2(r+p)x_0}} + \frac{r}{r+p} Q(p, x_R), \quad (41)$$

where \mathbb{C}_1 and \mathbb{C}_2 are constants which may be functions of p and x_R . We next use the boundary conditions in Eqs. (10) and (11) to evaluate these constants. Finally taking $x_0 = x_R$, we get

$$Q(p, x_R) = \frac{(r+p) e^{-\sqrt{2(r+p)x_R}}}{p+r e^{-\sqrt{2(r+p)x_R}}}. \quad (42)$$

The mean first passage time can be obtained simply as

$$\langle t_f \rangle = -\partial_p Q(p, x_R)|_{p \rightarrow 0} = \frac{1}{r} \left(e^{\sqrt{2r}x_R} - 1 \right), \quad (43)$$

which was first derived by Majumdar and Evans in [37]. The first passage time (under resetting) density can be exactly computed by inverting the Laplace inversion in Eq. (42). We refer the readers to Appendix A for the complete derivation. The final expression reads

$$P_R(t_f, x_R) = \left[\frac{r u_0 e^{-b_0 \sqrt{u_0}}}{1 - \frac{b_0}{2\sqrt{u_0}} e^{-b_0 \sqrt{u_0}}} \right] e^{-r(1-u_0)t_f} + H_r(t_f), \quad \text{with} \quad (44)$$

$$H_r(t_f) = \frac{e^{-rt_f}}{\pi} \int_0^\infty dw e^{-wt_f} \frac{w(r+w) \sin(\sqrt{2w}x_R)}{(r+w)^2 + r^2 - 2r(r+w) \cos(\sqrt{2w}x_R)} \quad (45)$$

where u_0 ($0 \leq u_0 \leq 1$) is a solution of the equation $u_0 = 1 - \exp(-\sqrt{u_0} b_0)$ and $b_0 = \sqrt{2r}x_R$. For $r = 0$, the first term in Eq. (44) vanishes. Performing integration over

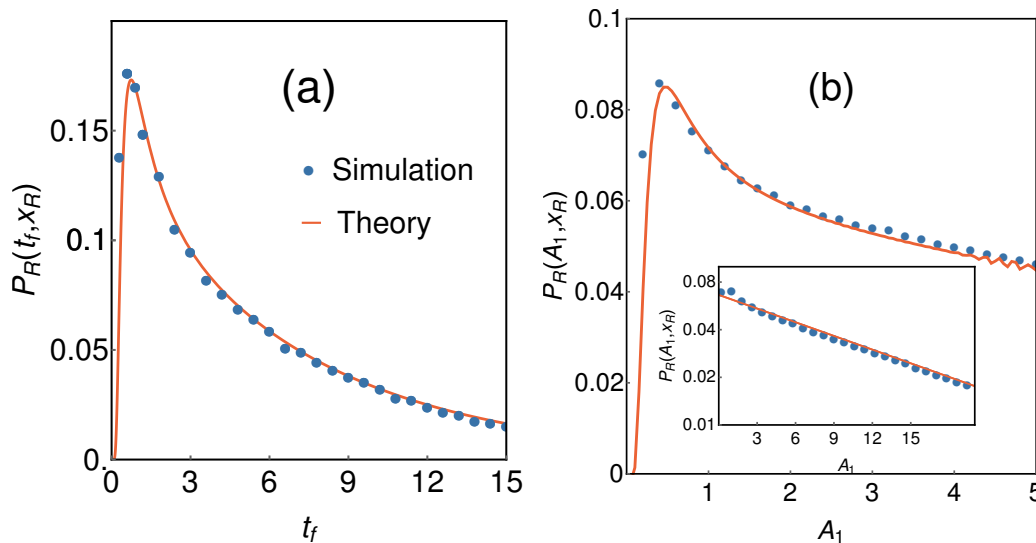


Figure 6. Left panel: analytical result for the distribution $P_R(t_f, x_R)$ in Eq. (44) and its comparison with the simulation. We have set $r = 0.5$ and $x_0 = x_R = 1.5$. Right panel: plot of the distribution $P_R(A_n, x_R)$ (solid line) for $n = 1$ by numerically inverting the Laplace transform $Q(p, x_R)$ in Eq. (54). We have compared it with the simulation data (circles). *Inset:* plot of the asymptotic form of $P_R(A_1, x_R)$ for large A_1 in Eq. (59) (solid line) and its comparison with the simulation results (circles). Parameters taken are $x_0 = x_R = 1.5$ and $r = 2$.

w in $H_r(t_f)$, we get

$$P_R(t_f, x_R) = \frac{1}{\sqrt{2\pi t_f^{3/2}}} \exp\left(-\frac{x_R^2}{2t_f}\right), \quad \text{for } r = 0 \quad (46)$$

which reduces to the well known result for Brownian motion [16]. On the other hand, in the large t limit, the first term in Eq. (44) dominates and the first-passage time distribution decays as $P_R(t_f, x_R) \sim e^{-r(1-u_0)t_f}$ [the long time behavior can also be understood from the extreme value statistics (see [37, 89]) and the survival probability [48]]. This is noteworthy since the tails of the FPT distribution are exponential while the underlying diffusion has power-law ($\sim t^{-3/2}$) first passage tails [16]. Simply put, resetting mechanism mitigates large time fluctuations that could induce delays. In fact, more the fluctuations, the better it works thus turning a marked drawback into a favourable advantage (see [77] for a very pedagogic viewpoint on this issue). For completeness, we have compared the analytic expression in Eq. (44) against the numerical simulations in Fig. 6 (left panel).

5.2. $n = 1$

Let us now turn to another exactly solvable case with $n = 1$. Recall that for this case, $A_1(x_0)$ represents the total area swept by the particle till it gets absorbed. To solve Eq.

(40) for $n = 1$, we make the following transformations:

$$\bar{Q}(p, x_0) = \frac{p^{2/3}}{\pi r 2^{1/3}} \left[\frac{Q(p, x_0)}{Q(p, x_R)} \right], \quad (47)$$

$$z = (2p)^{1/3} \left(x_0 + \frac{r}{p} \right). \quad (48)$$

Rewriting Eq. (40) in terms of these variables

$$\frac{\partial^2 \bar{Q}(p, z)}{\partial z^2} - z \bar{Q}(p, z) = -\frac{1}{\pi}. \quad (49)$$

The solution of this equation is given in terms of the Scorer's function $\text{Gi}(z)$ as [90, 91]

$$\bar{Q}(p, z) = \mathbb{C}_3 \text{Ai}(z) + \mathbb{C}_4 \text{Bi}(z) + \text{Gi}(z), \quad (50)$$

where $\text{Ai}(y)$ and $\text{Bi}(y)$ are Airy functions. Retracing back to the actual variables x_0 and $Q(p, x_0)$ in Eqs. (47) and (48), we get

$$Q(p, x_0) = \mathbb{C}_3 \text{Ai}(y_p(x_0)) + \mathbb{C}_4 \text{Bi}(y_p(x_0)) + \frac{\pi r 2^{1/3}}{p^{2/3}} Q(p, x_R) \text{Gi}(y_p(x_0)), \quad (51)$$

$$\text{with } y_p(x_0) = (2p)^{1/3} \left(x_0 + \frac{r}{p} \right). \quad (52)$$

The task now is to compute the constants \mathbb{C}_3 and \mathbb{C}_4 for which we use the boundary conditions in Eq. (10) and (11). Note that $\text{Bi}(y_p(x_0))$ diverges as $x_0 \rightarrow \infty$ which implies that $\mathbb{C}_4 = 0$ (see Eq. (11)). The other constant \mathbb{C}_3 follows from Eq. (10) as

$$\mathbb{C}_3(p, x_R) = \frac{1 - \frac{\pi r 2^{1/3}}{p^{2/3}} Q(p, x_R) \text{Gi}(y_p(0))}{\text{Ai}(y_p(0))}. \quad (53)$$

Inserting this form of $\mathbb{C}_3(p, x_R)$ in Eq. (51) and setting the initial position x_0 equal to the resetting position x_R , we get

$$Q(p, x_R) = \frac{\text{Ai}(y_p(x_R))}{\text{Ai}(y_p(0)) \mathcal{M}(p, x_R)}, \quad \text{where} \quad (54)$$

$$\mathcal{M}(p, x_R) = 1 + \frac{\pi r 2^{1/3}}{p^{2/3}} \left[\frac{\text{Ai}(y_p(x_R))}{\text{Ai}(y_p(0))} \text{Gi}(y_p(0)) - \text{Gi}(y_p(x_R)) \right]. \quad (55)$$

For $r = 0$, we have $\mathcal{M}(p, x_R) = 1$ and $y_p(x_R) = (2p)^{1/3} x_R$. Substituting these forms in Eq. (54) gives $Q(p, x_R) = \text{Ai}((2p)^{1/3} x_R) / \text{Ai}(0)$. This matches with the well-known result of Brownian motion in the absence of resetting [22, 23].

Moments of $A_1(x_R)$ can be obtained from $Q(p, x_R)$ using Eq. (6). One can, in principle, compute all the moments of $A_1(x_R)$ from Eq. (54). Here, we provide expressions for the first two moments:

$$\langle A_1(x_R) \rangle = \frac{x_R}{r} e^{\sqrt{2r} x_R}, \quad (56)$$

$$\langle A_1^2(x_R) \rangle = \frac{2e^{\sqrt{2r} x_R}}{r} \left[\frac{x_R^2}{r} \left(\frac{3}{4} + e^{\sqrt{2r} x_R} \right) + \frac{1}{r^2} - \frac{x_R^3}{2\sqrt{2r}} \right] - \frac{2}{r^3}. \quad (57)$$

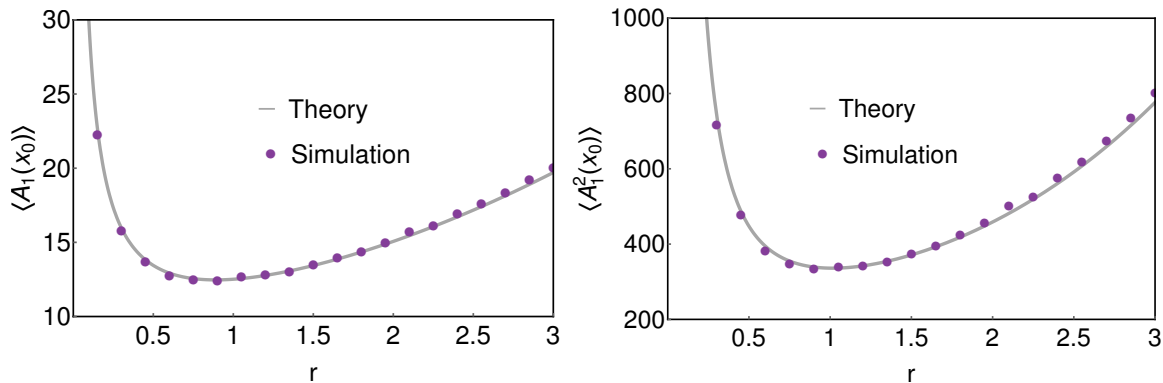


Figure 7. Comparison of the first two moments of the area $A_1(x_0)$ in Eqs. (56) and (57) with numerical simulation. We have taken $x_0 = x_R = 1.5$ for both plots.

In Fig. 7, we have plotted $\langle A_1(x_R) \rangle$ and $\langle A_1^2(x_R) \rangle$ as functions of the resetting rate r and compared against the results of simulation. It is worth remarking that the moments of $A_1(x_R)$ for the Brownian motion (without resetting) are infinite as was shown in [22]. Once again, the moments become finite under the resetting mechanism. Furthermore, we see that the moments exhibit non-monotonic dependence on r with a minimum at some optimal value of r^* . We later show that this non-monotonic dependence is a generic feature for all values of $n > -2$.

We now proceed to calculate the distribution of the area $A_1(x_R)$ by performing the inverse Laplace transformation of $Q(p, x_R)$ in Eq. (54). Performing inverse Laplace transformation for arbitrary p analytically turns out to be difficult. However, one can invert $Q(p, x_R)$ by performing the Bromwich integral numerically. In Fig. 6 (right panel) we compare thus numerically obtained $P_R(A_1, x_R)$ against simulation data. In order to make some analytic progress, we analyse $Q(p, x_R)$ in limit of small p (equivalently large A_1). For small p , $y_p(x_R) \rightarrow \infty$ as seen from Eq. (52) which in turn implies that the argument of $\text{Ai}(y_p(x_R))$ and $\text{Gi}(y_p(x_R))$ in Eqs. (54) and (55) become very large. We therefore approximate $\text{Ai}(y_p) \simeq \frac{e^{-\frac{2}{3}y_p^{3/2}}}{2\sqrt{\pi\sqrt{y_p}}}$ and $\text{Gi}(y_p) \simeq \frac{1}{\pi y_p}$ for large y_p and insert them in Eq. (54) to get an approximate expression for $Q(p, x_R)$ as

$$Q(p, x_R) \simeq \frac{1}{1 + p \frac{x_R}{r} e^{\sqrt{2r}x_R}}, \quad \text{as } p \rightarrow 0. \quad (58)$$

The inverse Laplace transformation yields an exponential distribution for $P_R(A_1, x_R)$ namely

$$P_R(A_1, x_R) \simeq \frac{r e^{-\sqrt{2r}x_R}}{x_R} \exp\left(-\frac{r e^{-\sqrt{2r}x_R}}{x_R} A_1\right). \quad (59)$$

We emphasise that this expression works only for $A_1 \gg \frac{x_R}{r} e^{\sqrt{2r}x_R}$. In Fig. 6 (inset of right panel), we have compared this analytical distribution with the same obtained from simulation. We see that there is a mismatch for the small values of A_1 . However,

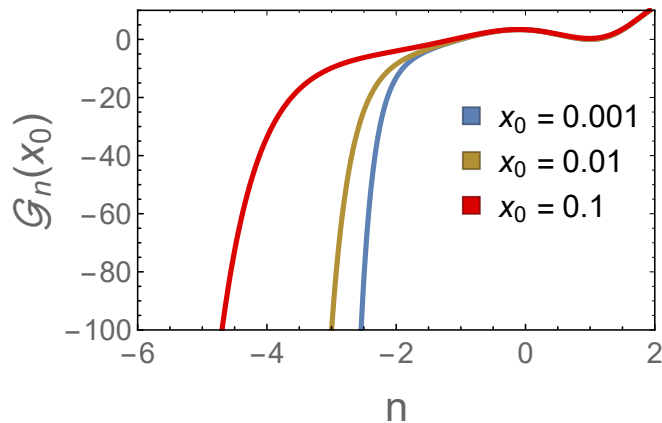


Figure 8. $\mathcal{G}_n(x_0)$ as a function of n for different values of x_0 in the limit $x_0 \rightarrow 0$.

the prediction becomes accurate as one goes to higher A_1 . We remark that while the distribution of A_1 for Brownian motion (without resetting) has power-law decay of the form $\sim A_1^{-4/3}$ as $A_1 \rightarrow \infty$ [22,23], it decays exponentially for $r > 0$ demonstrating again the typical behavior of resetting.

5.3. General n (> -2)

We now consider the statistics of $A_n(x_0) = \int_0^{t_f} [x(\tau)]^n d\tau$ for general values of n (> -2). For this, one has to solve the backward Fokker Planck Eq. (40) along with the boundary conditions in Eqs. (10) and (11). Solving Eq. (40) for arbitrary n and p turns out to be challenging. Here, we present some heuristic analysis that gives exactly the large- A_n behaviour of the distribution $P_R(A_n, x_R)$.

Numerically, we see that $P_R(A_n, x_0)$ decays exponentially for large A_n for all values of n . For $n = 0$ and $n = 1$, we were able to derive this explicitly. Motivated by these observations, we take the following ansatz:

$$P_R(A_n, x_0) \simeq \frac{e^{-A_n/a_n(x_0)}}{a_n(x_0)}, \quad \text{as } A_n \rightarrow \infty, \quad (60)$$

where $a_n(x_0)$ sets the decay-length for A_n . To answer the explicit form of $a_n(x_0)$, we first rewrite Eq. (60) in terms of the Laplace transformation $Q(p, x_0)$ as

$$Q(p, x_0) = \frac{1}{1 + p a_n(x_0)}, \quad (61)$$

which is valid only for small p (equivalently for large A_n). We next insert this form of $Q(p, x_0)$ in the backward Eq. (40) and up to leading order in p , we get

$$\frac{1}{2} \frac{d^2 a_n}{dx_0^2} - r a_n(x_0) + r a_n(x_R) = -x_0^n. \quad (62)$$

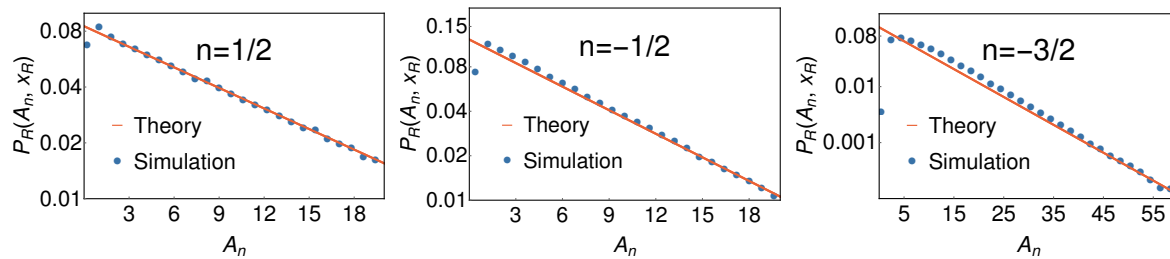


Figure 9. Plot of the distribution $P_R(A_n, x_R)$ in Eq. (60) and comparison with the results of simulation for $n = 1/2$ (left), $n = -1/2$ (middle) and $n = -3/2$ (right). Parameters taken are $x_0 = x_R = 1.5$ and $r = 2$.

Solving this equation using *Mathematica*, we find

$$a_n(x_0) = a_n(x_R) + \mathbb{C}_5 e^{-\sqrt{2r}x_0} + \mathbb{C}_6 e^{\sqrt{2r}x_0} + \mathcal{G}_n(x_0), \quad \text{with} \quad (63)$$

$$\mathcal{G}_n(x_0) = \text{Re} \left[\frac{e^{\sqrt{2r}x_0} \Gamma(1+n, \sqrt{2r}x_0) + (-1)^{-n} e^{-\sqrt{2r}x_0} \Gamma(1+n, -\sqrt{2r}x_0)}{(\sqrt{2r})^{n+2}} \right], \quad (64)$$

where $\text{Re}[\cdot]$ indicates the real part of $[\cdot]$. Recall that the function $\mathcal{G}_n(x_0)$ is the particular integral of Eq. (62) and we have taken its real part since the solution $a_n(x_0)$ has to be real. This is also true otherwise since $a_n(x_0)$ represents the mean of $A_n(x_0)$ which is always real.

It is easy to see that the function $\mathcal{G}_n(x_0)$ diverges for $n \leq -2$ as $x_0 \rightarrow 0$ (see Fig. 8). We later illustrate that this behaviour is not consistent with the boundary condition. In other words, the solution of $a_n(x_0)$ in Eq. (63) is not pertinent for $n \leq -2$. We now proceed to evaluate the constants \mathbb{C}_5 and \mathbb{C}_6 in Eq. (63) for which we use the boundary conditions given by Eqs. (10) and (11). The former condition gives $a_n(x_0 \rightarrow 0) = 0$. Using the second condition, we have $a_n(x_0 \rightarrow \infty) < \infty$ since the distribution $P_R(A_n, x_0)$ in Eq. (60) is finite for $x_0 \rightarrow \infty$. These two conditions evaluate the constants: $\mathbb{C}_5(p, x_R) = -a_n(x_R) - \mathcal{G}_n(0)$ and $\mathbb{C}_6(p, x_R) = 0$. Finally, setting $x_0 = x_R$ we get

$$a_n(x_R) = e^{\sqrt{2r}x_R} \mathcal{G}_n(x_R) - \mathcal{G}_n(0). \quad (65)$$

This expression of $a_n(x_R)$ along with $P_R(A_n, x_R)$ in Eq. (60) fully characterizes the distribution in the limit of large A_n . Our result is consistent with that for the cases $n = 0$ and $n = 1$ which we rigorously derived. We remark that for simple diffusion without resetting, the distribution of $A_n(x_R)$ exhibits power-law decay i.e., $P_0(A_n) \sim A_n^{-(n+3)/(n+2)}$ for large A_n as was shown by Majumdar and Meerson [22]. This behavior remarkably changes as we have shown here that there is a resetting induced exponential decay at least in the asymptotic limit. In Fig. 9, we have illustrated this large- A_n behaviour of $P_R(A_n, x_R)$ for $n = 1/2$ (left panel), $n = -1/2$ (middle panel) and $n = -3/2$ (right panel) and compared with numerical simulations. We observe an excellent agreement between analytical and simulation results for all the cases.

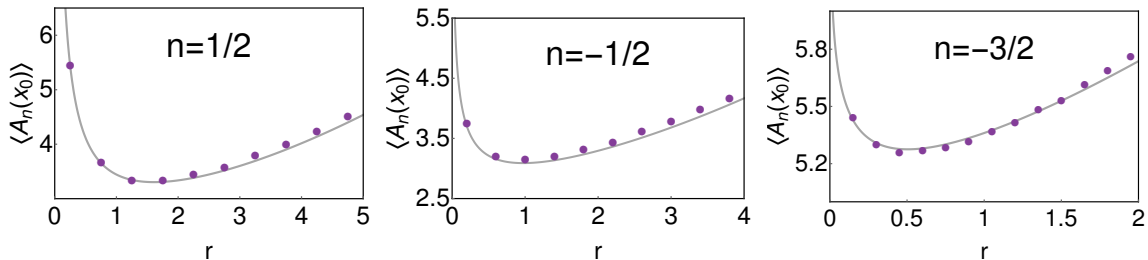


Figure 10. Plots of $\langle A_n(x_R) \rangle$ in Eq. (66) (shown by solid line) for $n = 1/2$ (left), $n = -1/2$ (middle) and $n = -3/2$ (right). The theoretical results (solid lines) provide an excellent agreement with the numerical simulations (circles). Parameters in this plot: $x_0 = x_R = 1$.

Interestingly, the decay length $a_n(x_R)$ in Eq. (65) also turns out to be the mean of $A_n(x_R)$ as stated above. This can be easily verified by rewriting the backward Eq. (40) in terms of $\langle A_n(x_0) \rangle$ which turns out to be same as for $a_n(x_0)$ in Eq. (62). Therefore, we have

$$\langle A_n(x_R) \rangle = e^{\sqrt{2r}x_R} \mathcal{G}_n(x_R) - \mathcal{G}_n(0), \quad (66)$$

where the function $\mathcal{G}_n(x_R)$ is given in Eq. (64). For $n = 0$ and $n = 1$, we correctly recover the results of the previous sections. In Fig. 10, we have compared the analytical expression of the mean $\langle A_n(x_R) \rangle$ with the results of simulation for $n = 1/2$ (left panel), $n = -1/2$ (middle panel) and $n = -3/2$ (right panel). The finiteness of the moments can again be attributed as a direct consequence of resetting. Moreover, the non-monotonic behaviour of the moments is clearly observed as in the case of $n = 0$ and $n = 1$.

6. Conclusion

In summary, we have characterized the statistical properties of various first passage Brownian functionals in the presence of resetting. Following the famous Feynman-Kac formalism, we presented a general approach that allows for the computation of the local time, residence time, area and other functionals of a Brownian trajectory that obeys overdamped Langevin dynamics and may also be subject to stochastic resetting. The process is observed till the first passage time t_f when the particle gets absorbed to the origin for the first time. The central step was to derive a backward differential Eq. (9) for the moment generating function of the functional. This equation was then extensively utilized to derive the exact formulae for the distributions and moments of the local time (T_{loc}) and residence time (T_{res}). Our study reveals that just like for t_f , the moments of T_{res} also display a non-monotonic dependence on the resetting rate r and exhibit minima at some optimal resetting rate.

We then turn our attention to the statistics of the functional $A_n(x_0) = \int_0^{t_f} d\tau [x(\tau)]^n$ for $n > -2$. The case of $n = 0$ simply represents the first-passage time t_f – the statistics of which is well understood now. Our central focus was on the non-zero values of n .

For $n = 1$, we again employed the backward Eq. (9) and obtained exact expression of the moment generating function. Utilizing this function, we derive the moments and asymptotic distribution of the area. For this case also, the moments exhibit a non-monotonic dependence on r with minima at some optimal rate r^* . Solving Eq. (9) for other values of n turns out to be difficult. Borrowing wisdom from $n = 0$ and $n = 1$ cases, we presented a heuristic analysis for the general n case which correctly captures the asymptotic form of the distribution of $A_n(x_0)$. For general n , we also derived the form of mean $A_n(x_0)$ which, once again, show non-monotonic dependence on r . The main conclusion can be summarized in the following way: Resetting renders the moments of general functional $A_n(x_0)$ finite for any $n > -2$ similar to the first passage time t_f (which is the $n = 0$ case). This is a clear consequence of resetting which removes detrimental realizations that take exceedingly large times to reach the target. Thus, under stochastic resetting, the overall process is completed faster and this feature seems to be quite universal.

Our results can be extended for drift-diffusion processes where drift plays a crucial role in determining the underlying first passage time density. It is known that resetting is detrimental in the high drift limit, while it can expedite the process completion when diffusion dominates over drift. These two phenomena are known to be separated by a resetting transition [92–94]. It would be interesting to study these functionals in these two limits and across the transition point.

Notably, the framework put forward herein is based on the assumption that the resetting is a Markov process. In simple words, resetting time density is exponential and thus memoryless. It would be challenging to extend the formalism under non-exponential resetting time densities. One approach could be to make use of the renewal structure which has been instrumental in connecting observable under resetting with the same in the absence of resetting. However, at this point it not immediately clear how to adapt to that approach for the first passage time functionals. We believe that answering these questions would further deepen our understanding of various first passage time functionals and their behavior in a more general set-up.

7. Acknowledgement

PS acknowledges support from the Department of Atomic Energy, Government of India, under project no.12-R&D-TFR-5.10-1100. AP acknowledges support from the Department of Atomic Energy, Government of India.

Appendix A. Derivation of Eq. (44)

In this appendix, we present the derivation for $P_R(t_f, x_R)$ which was announced in Eq. (44). Recall that the distribution in Laplace space is given by (see Eq. 42)

$$Q(p, x_R) = \frac{(r+p) e^{-\sqrt{2(r+p)x_R}}}{p+r e^{-\sqrt{2(r+p)x_R}}}. \quad (\text{A.1})$$

Formally, the inverse Laplace transform can be written in terms of the Bromwich integral as

$$P_R(t_f, x_R) = \frac{1}{2\pi i} \int_{\gamma_E - i\infty}^{\gamma_E + i\infty} dp e^{pt_f} Q(p, x_R). \quad (\text{A.2})$$

Here γ_E represents a vertical line in the complex plane such that all poles lie to its left (see Fig. A1). Plugging $Q(p, x_R)$ from Eq. (A.1), we notice that the integral in Eq. (A.3) has a branch point at $p = -r$ and a simple pole at $p_0 = -r(1 - u_0)$ with u_0 ($0 \leq u_0 \leq 1$) obeying the equation $u_0 = 1 - e^{-b_0\sqrt{u_0}}$ where $b_0 = \sqrt{2r}x_R$. Note that the pole p_0 lies in between $-r$ and 0. This motivates us to choose $\gamma_E = 0$ and consider contour of the form in Fig. A1 to evaluate Eq. (A.3).

Since, the integrand has a simple pole inside this contour, Cauchy's theorem states

$$\int_{\Gamma_1} + \int_{\Gamma_2} + \int_{\Gamma_3} + \int_{\Gamma_4} + \int_{\Gamma_5} + \int_{\Gamma_6} = \text{Residue of } e^{pt_f} Q(p, x_R) \text{ at } p_0. \quad (\text{A.3})$$

Note that $\int_{\Gamma_1} = P_R(t_f, x_R)$ is the required integral. We first compute the residue at $p = p_0$.

$$\text{Residue at } p_0 = \lim_{p \rightarrow p_0} [(p - p_0) e^{pt_f} Q(p, x_R)] \quad (\text{A.4})$$

$$= \left[\frac{ru_0 e^{-b_0\sqrt{u_0}}}{1 - \frac{b_0}{2\sqrt{u_0}} e^{-b_0\sqrt{u_0}}} \right] e^{-r(1-u_0)t_f}. \quad (\text{A.5})$$

Next we proceed to compute the contribution of integrals across different paths in Eq. (A.3). Recall that the real part of p along Γ_2 and Γ_6 is negative and in the limit $|p| \rightarrow \infty$, this contribution becomes zero. On the other hand, for Γ_4 , we substitute $p = -r + \epsilon e^{i\theta}$ and take $\epsilon \rightarrow 0^+$ limit. The integrand, in this limit, becomes exactly zero, i.e. $\int_{\Gamma_4} = 0$. Hence, we only have to evaluate integrals along Γ_3 and Γ_5 . To evaluate \int_{Γ_3} , we substitute $p = -r + we^{i\pi}$ to obtain

$$\int_{\Gamma_3} = \frac{1}{2\pi i} \int_0^\infty dw e^{-(r+w)t_f} \frac{we^{-i\sqrt{2wx_R}}}{r+w - re^{-i\sqrt{2wx_R}}}. \quad (\text{A.6})$$

Similarly, for \int_{Γ_5} , we substitute $p = -r + we^{-i\pi}$ to get

$$\int_{\Gamma_5} = -\frac{1}{2\pi i} \int_0^\infty dw e^{-(r+w)t_f} \frac{we^{i\sqrt{2wx_R}}}{r+w - re^{i\sqrt{2wx_R}}}. \quad (\text{A.7})$$

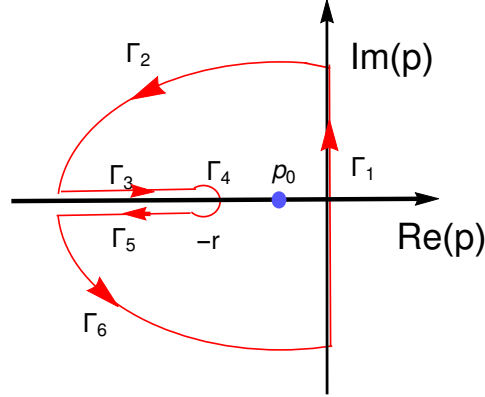


Figure A1. Contour for the Bromwich integral in Eq. (A.3)

Inserting all these contributions in Eq. (A.3) and performing some algebraic simplifications, we find

$$P_R(t_f, x_R) = \left[\frac{ru_0 e^{-b_0\sqrt{u_0}}}{1 - \frac{b_0}{2\sqrt{u_0}} e^{-b_0\sqrt{u_0}}} \right] e^{-r(1-u_0)t_f} + H_r(t_f), \quad \text{with} \quad (\text{A.8})$$

$$H_r(t_f) = \frac{e^{-rt_f}}{\pi} \int_0^\infty dw e^{-wt_f} \frac{w(r+w) \sin(\sqrt{2wx_R})}{(r+w)^2 + r^2 - 2r(r+w) \cos(\sqrt{2wx_R})}. \quad (\text{A.9})$$

This result has been quoted in Eq. (44)

References

- [1] Majumdar, S.N., 2007. Brownian functionals in physics and computer science. In *The Legacy Of Albert Einstein: A Collection of Essays in Celebration of the Year of Physics* (pp. 93-129).
- [2] Kac, M 1949. On distributions of certain Wiener functionals. *Transactions of the American Mathematical Society*, 65, 1-13
- [3] Seifert, U., 2012. Stochastic thermodynamics, fluctuation theorems and molecular machines. *Reports on progress in physics*, 75(12), p.126001.
- [4] Chernyak, V.Y., Chertkov, M. and Jarzynski, C., 2006. Path-integral analysis of fluctuation theorems for general Langevin processes. *Journal of Statistical Mechanics: Theory and Experiment*, 2006(08), p.P08001.
- [5] Lévy, P. and Loève, M., 1965. *Processus stochastiques et mouvement brownien* (pp. 299-304). Paris: Gauthier-Villars.
- [6] Knight, F.B., 1969. Brownian local times and taboo processes. *Transactions of the American Mathematical Society*, 143, pp.173-185.
- [7] Feller, W., 2008. *An introduction to probability theory and its applications* (Vol. 2). John Wiley & Sons.
- [8] Comtet, A., Desbois, J. and Majumdar, S.N., 2002. The local time distribution of a particle diffusing on a graph. *Journal of Physics A: Mathematical and General*, 35(47), p.L687.
- [9] Csorgo, M., Shi, Z. and Yor, M., 1999. Some asymptotic properties of the local time of the uniform empirical process. *Bernoulli*, 5(6), pp.1035-1058.
- [10] Singh, P. and Kundu, A., 2021. Local time for run and tumble particle. *Physical Review E*, 103(4), p.042119.

- [11] Agmon, N., 1984. Residence times in diffusion processes. *The Journal of chemical physics*, 81(8), pp.3644-3647.
- [12] Berezhkovskii, A.M., Zalozj, V. and Agmon, N., 1998. Residence time distribution of a Brownian particle. *Physical Review E*, 57(4), p.3937.
- [13] Nguyen, B.T. and Grebenkov, D.S., 2010. A spectral approach to survival probabilities in porous media. *Journal of Statistical Physics*, 141(3), pp.532-554.
- [14] Pal, A., Castillo, I.P. and Kundu, A., 2019. Motion of a Brownian particle in the presence of reactive boundaries. *Physical Review E*, 100(4), p.042128.
- [15] Majumdar, S.N. and Comtet, A., 2002. Local and occupation time of a particle diffusing in a random medium. *Physical review letters*, 89(6), p.060601.
- [16] S. Redner, *A Guide to First-Passage Processes* (Cambridge University Press 2001).
- [17] Grebenkov, D.S., 2007. Residence times and other functionals of reflected Brownian motion. *Physical Review E*, 76(4), p.041139.
- [18] Sabhapandit, S., Majumdar, S.N. and Comtet, A., 2006. Statistical properties of functionals of the paths of a particle diffusing in a one-dimensional random potential. *Physical Review E*, 73(5), p.051102.
- [19] Singh, P. 2022, Extreme value statistics and arcsine laws for heterogeneous diffusion processes, arXiv:2112.00088 (accepted to *Phy. Rev. E*).
- [20] Louchard, G., 1984. Kac's formula, Levy's local time and Brownian excursion. *Journal of Applied Probability*, 21(3), pp.479-499.
- [21] Singh, P., and Kundu, A., 2019, Generalised 'Arcsine' laws for run-and-tumble particle in one dimension, *J.Stat.Mech*, 083205.
- [22] Majumdar, S.N. and Meerson, B., 2020. Statistics of first-passage Brownian functionals. *Journal of Statistical Mechanics: Theory and Experiment*, 2020(2), p.023202.
- [23] Kearney, M.J. and Majumdar, S.N., 2005. On the area under a continuous time Brownian motion till its first-passage time. *Journal of Physics A: Mathematical and General*, 38(19), p.4097.
- [24] Bray, A.J., Majumdar, S.N. and Schehr, G., 2013. Persistence and first-passage properties in nonequilibrium systems. *Advances in Physics*, 62(3), pp.225-361.
- [25] Kearney, M.J., 2004. On a random area variable arising in discrete-time queues and compact directed percolation. *Journal of Physics A: Mathematical and General*, 37(35), p.8421.
- [26] Prellberg, T. and Brak, R., 1995. Critical exponents from nonlinear functional equations for partially directed cluster models. *Journal of statistical physics*, 78(3), pp.701-730.
- [27] Majumdar, S.N. and Kearney, M.J., 2007. Inelastic collapse of a ball bouncing on a randomly vibrating platform. *Physical Review E*, 76(3), p.031130.
- [28] Dhar, D. and Ramaswamy, R., 1989. Exactly solved model of self-organized critical phenomena. *Physical Review Letters*, 63(16), p.1659.
- [29] Abundo, M., 2013. On the first-passage area of a one-dimensional jump-diffusion process. *Methodology and Computing in Applied Probability*, 15(1), pp.85-103.
- [30] Abundo, M. and Del Vescovo, D., 2017. On the joint distribution of first-passage time and first-passage area of drifted Brownian motion. *Methodology and Computing in Applied Probability*, 19(3), pp.985-996.
- [31] Abundo, M. and Furia, S., 2019. Joint Distribution of First-Passage Time and First-Passage Area of Certain Lévy Processes. *Methodology and Computing in Applied Probability*, 21(4), pp.1283-1302.
- [32] Kearney, M.J. and Martin, R.J., 2021. Statistics of the first passage area functional for an Ornstein-Uhlenbeck process. *Journal of Physics A: Mathematical and Theoretical*, 54(5), p.055002.
- [33] Abundo, M., 2021. The first-passage area of Ornstein-Uhlenbeck process revisited. *Stochastic Analysis and Applications*, pp.1-19.
- [34] Hammersley, J.M., 2020. On the statistical loss of long-period comets from the solar system. II. In *Contributions to Astronomy, Meteorology, and Physics* (pp. 17-78). University of California

Press.

- [35] Dean, D.S. and Majumdar, S.N., 2001. The exact distribution of the oscillation period in the underdamped one-dimensional Sinai model. *Journal of Physics A: Mathematical and General*, 34(49), p.L697.
- [36] Evans M R, Majumdar S N and Schehr G 2020 *J. Phys. A: Math. Theor.* 53 193001
- [37] Evans, M.R. and Majumdar, S.N., 2011. Diffusion with stochastic resetting. *Physical review letters*, 106(16), p.160601.
- [38] Evans, M.R. and Majumdar, S.N., 2011. Diffusion with optimal resetting. *Journal of Physics A: Mathematical and Theoretical*, 44(43), p.435001.
- [39] Reuveni, S., Urbakh, M. and Klafter, J., 2014. Role of substrate unbinding in Michaelis–Menten enzymatic reactions. *Proceedings of the National Academy of Sciences*, 111(12), pp.4391-4396.
- [40] Robin, T., Reuveni, S. and Urbakh, M., 2018. Single-molecule theory of enzymatic inhibition. *Nature communications*, 9(1), p.779.
- [41] Roldan, E., Lisica, A., Sanchez-Taltavull, D. and Grill, S.W., 2016. Stochastic resetting in backtrack recovery by RNA polymerases. *Physical Review E*, 93(6), p.062411.
- [42] Budnar, S., Husain, K.B., Gomez, G.A., Naghibosadat, M., Varma, A., Verma, S., Hamilton, N.A., Morris, R.G. and Yap, A.S., 2019. Anillin promotes cell contractility by cyclic resetting of RhoA residence kinetics. *Developmental cell*, 49(6), pp.894-906.
- [43] Majumdar, S.N., Sabhapandit, S. and Schehr, G., 2015. Dynamical transition in the temporal relaxation of stochastic processes under resetting. *Physical Review E*, 91(5), p.052131.
- [44] Pal, A., 2015. Diffusion in a potential landscape with stochastic resetting. *Physical Review E*, 91(1), p.012113.
- [45] Eule, S. and Metzger, J.J., 2016. Non-equilibrium steady states of stochastic processes with intermittent resetting. *New Journal of Physics*, 18(3), p.033006.
- [46] Nagar, A. and Gupta, S., 2016. Diffusion with stochastic resetting at power-law times. *Physical Review E*, 93(6), p.060102.
- [47] Pal, A., Kundu, A. and Evans, M.R., 2016. Diffusion under time-dependent resetting. *Journal of Physics A: Mathematical and Theoretical*, 49(22), p.225001.
- [48] Pal, A., Chatterjee, R., Reuveni, S. and Kundu, A., 2019. Local time of diffusion with stochastic resetting. *Journal of Physics A: Mathematical and Theoretical*, 52(26), p.264002.
- [49] Den Hollander, F., Majumdar, S.N., Meylahn, J.M. and Touchette, H., 2019. Properties of additive functionals of Brownian motion with resetting. *Journal of Physics A: Mathematical and Theoretical*, 52(17), p.175001.
- [50] Bressloff, P.C., 2020. Occupation time of a run-and-tumble particle with resetting. *Physical Review E*, 102(4), p.042135.
- [51] Méndez, V. and Campos, D., 2016. Characterization of stationary states in random walks with stochastic resetting. *Physical Review E*, 93(2), p.022106.
- [52] Pal, A., Reuveni, S. and Rahav, S., 2021. Thermodynamic uncertainty relation for systems with unidirectional transitions. *Physical Review Research*, 3(1), p.013273.
- [53] Luby, M., Sinclair, A. and Zuckerman, D., 1993. Optimal speedup of Las Vegas algorithms. *Information Processing Letters*, 47(4), pp.173-180.
- [54] Hamlin, P., Thrasher, W.J., Keyrouz, W. and Mascagni, M., 2019. Geometry entrapment in Walk-on-Subdomains. *Monte Carlo Methods and Applications*, 25(4), pp.329-340.
- [55] Kusmierz, L., Majumdar, S.N., Sabhapandit, S. and Schehr, G., 2014. First order transition for the optimal search time of Lévy flights with resetting. *Physical review letters*, 113(22), p.220602.
- [56] Pal, A., Kuśmierz, L. and Reuveni, S., 2020. Search with home returns provides advantage under high uncertainty. *Physical Review Research*, 2(4), p.043174.
- [57] Montanari, A. and Zecchina, R., 2002. Optimizing searches via rare events. *Physical review letters*, 88(17), p.178701.
- [58] Ray, A., Pal, A., Ghosh, D., Dana, S.K. and Hens, C., 2021. Mitigating long transient time in deterministic systems by resetting. *Chaos: An Interdisciplinary Journal of Nonlinear Science*,

- 31(1), p.011103.
- [59] Mercado-Vasquez, G. and Boyer, D., 2018. Lotka–volterra systems with stochastic resetting. *Journal of Physics A: Mathematical and Theoretical*, 51(40), p.405601.
 - [60] da Silva, T.T. and Fragoso, M.D., 2021. Diffusion with stochastic resetting of interacting particles emerging from a model of population genetics. *Journal of Physics A: Mathematical and Theoretical*, 55(1), p.014003.
 - [61] Boudali, O. and Economou, A., 2012. Optimal and equilibrium balking strategies in the single server Markovian queue with catastrophes. *European Journal of Operational Research*, 218(3), pp.708-715.
 - [62] Chao, X., 1995. A queueing network model with catastrophes and product form solution. *Operations Research Letters*, 18(2), pp.75-79
 - [63] Bonomo, O.L., Pal, A. and Reuveni, S., 2021. Mitigating long queues and waiting times with service resetting. arXiv preprint arXiv:2111.02097.
 - [64] Stojkoski, V., Jolajoski, P., Pal, A., Sandev, T., Kocarev, L. and Metzler, R., 2021. Income inequality and mobility in geometric Brownian motion with stochastic resetting: theoretical results and empirical evidence of non-ergodicity. arXiv preprint arXiv:2109.01822. To appear in *Phil. Transc. A*.
 - [65] Stojkoski, V., Sandev, T., Kocarev, L. and Pal, A., 2021. Geometric Brownian Motion under Stochastic Resetting: A Stationary yet Non-ergodic Process. *Phys. Rev. E* 104(1), 014121 (2021).
 - [66] Gabaix, X., Lasry, J.M., Lions, P.L. and Moll, B., 2016. The dynamics of inequality. *Econometrica*, 84(6), pp.2071-2111
 - [67] Tal-Friedman, O., Pal, A., Sekhon, A., Reuveni, S. and Roichman, Y., 2020. Experimental realization of diffusion with stochastic resetting. *J. Phys. Chem. Lett.* 2020, 11, 17, 7350–7355
 - [68] Besga, B., Bovon, A., Petrosyan, A., Majumdar, S.N. and Ciliberto, S., 2020. Optimal mean first-passage time for a Brownian searcher subjected to resetting: experimental and theoretical results. *Physical Review Research*, 2(3), p.032029.
 - [69] Faisant F, Besga B, Petrosyan A, Ciliberto S and Majumdar S N 2021 preprint arXiv:2106.09113. *J. Stat. Mech.* (2021) 113203
 - [70] Durang, X., Henkel, M. and Park, H., 2014. The statistical mechanics of the coagulation–diffusion process with a stochastic reset. *Journal of Physics A: Mathematical and Theoretical*, 47(4), p.045002.
 - [71] Majumdar, S.N., Sabhapandit, S. and Schehr, G., 2015. Dynamical transition in the temporal relaxation of stochastic processes under resetting. *Physical Review E*, 91(5), p.052131.
 - [72] Pal, A. and Prasad, V.V., 2019. First passage under stochastic resetting in an interval. *Physical Review E*, 99(3), p.032123.
 - [73] S. Ray, Space-dependent diffusion with stochastic resetting: A first-passage study, *J. Chem. Phys.* 153, 234904 (2020).
 - [74] Majumdar, S.N., Mori, F., Schawe, H. and Schehr, G., 2021. Mean perimeter and area of the convex hull of a planar Brownian motion in the presence of resetting. *Physical Review E*, 103(2), p.022135.
 - [75] Singh, P. and Pal, A., 2021. Extremal statistics for stochastic resetting systems. *Physical Review E*, 103(5), p.052119.
 - [76] Singh, R.K., Metzler, R. and Sandev, T., 2020. Resetting dynamics in a confining potential. *Journal of Physics A: Mathematical and Theoretical*, 53(50), p.505003.
 - [77] Pal, A., Kostinski, S. and Reuveni, S., 2022. The inspection paradox in stochastic resetting. *Journal of Physics A: Mathematical and Theoretical*, 55, p.021001. arXiv preprint arXiv:2108.07018.
 - [78] Pal, A., Eliazar, I. and Reuveni, S., 2019. First passage under restart with branching. *Physical review letters*, 122(2), p.020602.
 - [79] Pal, A. and Reuveni, S., 2017. First passage under restart. *Physical review letters*, 118(3), p.030603.
 - [80] Reuveni, S., 2016. Optimal stochastic restart renders fluctuations in first passage times universal. *Physical review letters*, 116(17), p.170601.

- [81] A. Chechkin and I. M. Sokolov, Random Search with Resetting: A Unified Renewal Approach, *Phys. Rev. Lett.* 121, 050601 (2018).
- [82] Kusmierz, L. and Gudowska-Nowak, E., 2015. Optimal first-arrival times in Lévy flights with resetting. *Physical Review E*, 92(5), p.052127.
- [83] Bhat, U., De Bacco, C. and Redner, S., 2016. Stochastic search with Poisson and deterministic resetting. *Journal of Statistical Mechanics: Theory and Experiment*, 2016(8), p.083401.
- [84] Chen, H., Li, G. and Huang, F., 2021. First passage in discrete-time absorbing Markov chains under stochastic resetting. *arXiv preprint arXiv:2111.01330*.
- [85] Falcón-Cortés, A., Boyer, D., Giuggioli, L. and Majumdar, S.N., 2017. Localization transition induced by learning in random searches. *Physical review letters*, 119(14), p.140603.
- [86] Singh, P., 2020. Random acceleration process under stochastic resetting. *Journal of Physics A: Mathematical and Theoretical*, 53(40), p.405005.
- [87] Capała, K. and Dybiec, B., 2021. Random acceleration process on finite intervals under stochastic restarting. *Journal of Statistical Mechanics: Theory and Experiment*, 2021(8), p.083216.
- [88] Belan, S., 2018. Restart could optimize the probability of success in a Bernoulli trial. *Physical review letters*, 120(8), p.080601.
- [89] Majumdar, S.N., Pal, A. and Schehr, G., 2020. Extreme value statistics of correlated random variables: a pedagogical review. *Physics Reports*, 840, pp.1-32.
- [90] NIST Digital Library of Mathematical Functions, F. W. J. Olver, A. B. Olde Daalhuis, D. W. Lozier, B. I. Schneider, R. F. Boisvert, C. W. Clark, B. R. Miller, B. V. Saunders, H. S. Cohl, and M. A. McClain
- [91] Abramowitz, M., Stegun, I. A. (1965). *Handbook of Mathematical Functions: With Formulas, Graphs, and Mathematical Tables*. New York: Dover.
- [92] Ray, S., Mondal, D. and Reuveni, S., 2019. Peclet number governs transition to acceleratory restart in drift-diffusion. *Journal of Physics A: Mathematical and Theoretical*, 52(25), p.255002.
- [93] Ahmad, S., Nayak, I., Bansal, A., Nandi, A. and Das, D., 2019. First passage of a particle in a potential under stochastic resetting: A vanishing transition of optimal resetting rate. *Physical Review E*, 99(2), p.022130.
- [94] Pal, A. and Prasad, V.V., 2019. Landau-like expansion for phase transitions in stochastic resetting. *Physical Review Research*, 1(3), p.032001.